The Stereostructure of Porphyra-334: An Experimental and Calculational NMR Investigation. Evidence for an Efficient 'Proton Sponge'

by **Manfred Klisch**[a]), **Peter Richter**[a]), **Ralph Puchta**[b]), **Donat-P. Häder**[a]), and **Walter Bauer***[c])

[a]) Chair of Plant Ecophysiology, University of Erlangen-Nuremberg, Staudtstrasse 5, D-91058 Erlangen

[b]) Computer Chemistry Center, Nägelsbachstrasse 25, D-91052 Erlangen

[c]) Institute of Organic Chemistry, University of Erlangen-Nuremberg, Henkestrasse 42, D-91054 Erlangen (e-mail: bauer@chemie.uni-erlangen.de)

Dedicated to Prof. Dr. *Jürgen Sauer*, Institute of Organic Chemistry, University of Regensburg, on the occasion of his 75th birthday

The mycosporine-like amino acid (MAA) porphyra-334 (**1**) is subjected to extensive ^{1}H- and ^{13}C-NMR analysis as well as to density-functional-theory (DFT) calculations. All ^{1}H- and ^{13}C-NMR signals of **1** are assigned, as well as the resonances of prochiral proton pairs. This is achieved by 500-MHz standard COSY, HMQC, and HMBC experiments, as well as by one-dimensional (DPFGSE-NOE) and two-dimensional (NOESY) NOE experiments. Diffusion measurements (DOSY) confirm that **1** is monomeric in D_2O solution. DFT Calculations yield ^{13}C-NMR chemical shifts which are in good agreement for species **6** which is the imino N-protonated form of **1**. An exceptionally high proton affinity of 265.7 kcal/mol is calculated for **1**, indicating that **1** may behave as a very powerful 'proton sponge' of comparable strength as synthetic systems studied so far. Predictions of ^{13}C-NMR chemical shifts by the 'NMRPredict' software are in agreement with the DFT data. The absolute configuration at the ring stereogenic center of **1** is concluded to be (*S*) from NOE data as well as from similarities with the absolute configuration (*S*) found in mycosporine-glycine **16**. This supports the assumption that **1** is biochemically derived from 3,3-*O*-didehydroquinic acid (**17**). The data obtained question the results recently published by a different research group claiming that the configuration at the imino moiety of **1** is (*Z*), rather than (*E*) as established by the here presented study.

Introduction. – Exposure to UV radiation may cause skin cancer [1] and photoaging of the skin. Nevertheless, in many industrialized countries, people continue to expose themselves voluntarily to solar radiation to gain a 'healthy' appearance. Thus, UV sunscreens are an important health issue and of great economical importance. Although there are several synthetic organic sunscreens on the market, there are concerns in the public about possible adverse effects that might be caused by these compounds. This leads to the interest in natural UV-absorbing compounds.

Among natural UV-absorbing compounds, mycosporine-like amino acids (MAAs) are an interesting group with respect to their high molar extinction coefficients mainly in the UV-A range (*e.g.*, $\varepsilon = 42300$ at 334 nm for porphyra-334 [2]), and the high photostability of certain MAAs, *e.g.*, porphyra-334 [3–5].

The MAA porphyra-334 (**1**) was identified in 1979 [2], and it is common among marine algae, most frequently and at high concentrations in red algae such as *Porphyra* ssp. [6–8]. This MAA has low quantum yields for fluorescence emission, intersystem

crossing, and photolysis [4] and dissipates *ca.* 97% of the absorbed energy as heat to the medium [5]. A UV-protective suntan lotion has been prepared with porphyra-334 (**1**) contained in liposomes and was found to be superior to a lotion containing a combination of synthetic UV sunscreens although its UV absorption was lower at the applied concentration of **1** [9]. UV-Absorbing compounds from *Porphyra yezoensis* were found to block very efficiently the formation of thymine dimers, an important form of UV-induced DNA damage. For this protective effect, some kind of energy transfer from excited states of thymine to MAA molecules was proposed; however, the exact mechanism is unclear [10]. There are also effects of **1** other than UV absorption that are related to oxygen metabolism. Some MAAs exhibit antioxidant activity, *e.g.*, mycosporine-glycine [11]. Although imino-MAAs such as porphyra-334 (**1**) are generally thought to be oxidatively more inert [12], an industrial patent claims that **1** improves oxygen uptake in human skin cells [13].

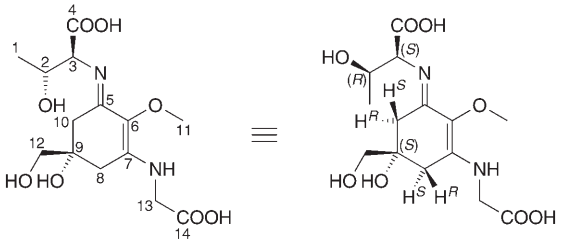

1[1])

Despite the ongoing research on photochemical properties and physiological roles of porphyra-334 (**1**), the absolute configuration of the molecule has not been determined. In this study, we applied a wide range of NMR techniques and calculations to provide further structural information on **1**[1]) that will help to interpret the interactions of the molecule in biological systems.

Experimental. – 1. *Extraction and Purification of Porphyra-334* (=*2-{[(1*E*)-3-[(Carboxymethyl)-amino]-5-hydroxy-5-(hydroxymethyl)-2-methoxycyclohex-2-en-1-ylidene]amino}-3-hydroxybutanoic Acid* (IUPAC name generated by ACD ChemSketch; **1**). Dried Nori (*Porphyra haitaiensis*) was briefly rehydrated with H_2O (10 ml/g) and extracted after addition of 100% EtOH (40 ml/g) for 2 h at r.t. The extract was filtered and concentrated at 45° under streaming air. The residue was extracted with ligroin, redissolved in H_2O and passed through a short column of *Dowex-W50-X4* beads. The column was washed with H_2O and eluted with 0.5N HCl. The eluate fractions containing UV-absorbing compounds were lyophilized. The combined residues were redissolved in H_2O and the soln. was applied to HPLC (*LiChrospher RP-18 100* (5 μm, 125 × 4 mm i.d.; *Merck KGaA*, Germany), isocratic 0.4% AcOH/H_2O flow 2 ml/min). The fractions containing **1** were lyophilized. The combined residues were redissolved in H_2O and the soln. was applied to HPLC (isocratic 0.02%, AcOH/H_2O, flow 2 ml/min). The fractions containing **1** were lyophilized. The combined residues were redissolved in MeOH and the soln. was divided into small portions. The MeOH was evaporated in a *Speedvac*, and the vials were sealed under N_2 and stored at −20°.

2. *NMR Spectroscopy.* NMR Samples of **1** were prepared as *ca.* 0.01M degassed solns. in D_2O. An external reference of a diluted soln. of acetone in D_2O was used: δ(H) 2.09, δ(C) 28.10. NMR Spectra:

---

[1]) H^R and H^S are prochiral H-atoms, *i.e.*, $H^{pro\text{-}R}$ and $H^{pro\text{-}S}$, respectively; short forms such as 10^R or 10^S stand for $H^{pro\text{-}R}$–C(10) or $H^{pro\text{-}S}$–C(10), respectively. Arbitrary numbering.

Jeol Alpha-500 spectrometer (^{1}H at 500 MHz, 11.7 T) at +25° and the standard *Jeol* software (version 2.00 of the *Alpha* 'EDL' program); δ in ppm, J in Hz. 1D ^{13}C-NMR Spectrum of *Figs. 2* and *3:* multinuclear 5-mm probehead; pulse width 6.0 μs (=60°), spectral width 33898 Hz, 32 k complex data points, 14180 scans, acquisition time 0.97 s, relaxation delay 3.0 s, exponential line broadening with BF = 1.5 Hz. ^{1}H-NMR and NOE Spectra and diffusion measurements: inverse probehead with actively shielded gradient coils (except: 2D-NOESY of *Fig. 5:* inverse probehead without gradient coils); typical 90° pulse widths 6.5 μs (^{1}H) and 15.5 μs (^{13}C). 1D ^{1}H-NMR Spectrum of the 2D plots: spectral width 4390 Hz, 16 k complex data points, pulse width 4.0 μs, 540 scans, acquisition time 3.7 s, relaxation delay 2.0 s, exponential line broadening with BF = 0.1 Hz.

Parameters of the COSY experiment (*Fig. 1*): standard COSY pulse sequence [14], pulsed-field-gradient mode [15], gradient strength 14 G/cm, 512 complex data points in t_2, zero-filled to 1024, spectral width in f_2 and f_1 2392 Hz, 8 scans per t_1 increment, acquisition time 0.214 s, relaxation delay 1.5 s, 256 t_1 increments, zero-filled to 512, unshifted sine bell window in t_1 and t_2, magnitude-mode recording and presentation. No symmetrization procedure was applied. Overall measurement time: 1.0 h.

Parameters of the HMQC experiment (*Fig. 2*): standard HMQC pulse sequence [16], pulsed-field-gradient mode [15], gradient strengths 56 and 28 G/cm, resp., 512 complex points in t_2, spectral width in f_2 2392 Hz, 8 scans per t_1 increment, acquisition time 0.214 s, relaxation delay 1.5 s, spectral width in f_1 21459 Hz, 512 t_1 increments, zero-filled to 1024, GARP decoupling for ^{13}C during acquisition, exponential window (4 Hz) in t_2, Gaussian window in t_1, magnitude-mode recording and presentation. Overall measurement time: 2.0 h.

Parameters of the HMBC experiment (*Fig. 3*): standard HMBC pulse sequence [17], pulsed-field-gradient mode [15]. Parameters as given above for *Fig. 2*, except for 64 scans per t_1 increment, relaxation delay 2.7 s, ^1J-filtering delay set to 3.7 ms, equivalent to 135 Hz, $^{2,3}J$-evolution delay set to 45 ms, equivalent to $^{2,3}J$(H,C) = 11 Hz, magnitude-mode recording and presentation. Overall measurement time: 13.5 h.

Parameters of the 1D NOE measurements (*Fig. 4, b* and *c*): DPFGSE-NOE sequence [18], spectral width 4390 Hz, 16 k complex data points, 2880 scans per irradiation point, acquisition time 3.7 s, relaxation delay 2.0 s, NOE-buildup delay 500 ms, gradient strengths 14/6/4/-4% (100% = 140 G/cm), gradient duration 1 ms each, selective Gauss pulse 40 ms, exponential line broadening with BF = 1.0 Hz. *Fig. 4, d:* same as for *Fig. 4, b* and *c*, except for 6976 scans, exponential line broadening with BF = 2.0 Hz.

Parameters of the NOESY experiment (*Fig. 5*): D_2O soln., +25°, inverse probehead, phase-sensitive mode, standard NOESY pulse sequence [19], spectral width in f_1 and f_2 2404 Hz, 512 complex data points in t_2, zero-filled to 1024, 256 increments in t_1, zero-filled to 512, 128 scans per t_1 increment, acquisition time 0.22 s, relaxation delay 2.0 s, 90° pulse width 6.5 μs, mixing time 500 ms, exponential window in t_1 (CBF = 4 Hz) and in t_2 (BF = 2 Hz); overall measurement time: 25 h.

Diffusion (PGSE) measurements (*Fig. 6*): BPP-LED-pulse sequence (BPP-LED = bipolar pulse longitudinal encoding decoding or bipolar pulse longitudinal eddy current delay) [20]. Temperature + 30.0°, spectral width 2619 Hz, 8k complex data points, 128 scans per gradient step, gradient duration 1 ms, diffusion delay 50 ms, 4 dummy scans, acquisition time 3.1 s, relaxation delay 3.0 s, maximum gradient strength 0.9 T/m. A total of 32 separate spectra with increasing gradients proportional to G^2 were recorded. Overall measurement time: 7.0 h. Data processing was achieved by using the *Jeol-Alpha* software for T_2 relaxation time analysis. In the graphical presentation of *Fig. 6* (*Stejskal-Tanner* plot [21]), the decay of the HDO signal was taken as an internal reference with a hydrodynamic radius r_H of H_2O = 0.765 Å (*via* the *Stokes–Einstein* equation). Along with the slope of the decay of the Me(1) signal of porphyra-334 (**1**), this yields a hydrodynamic radius 4.39 Å for **1**.

Assignments for **1** (arbitrary numbering, see *Formula*): ^{1}H-NMR[1]) (D_2O, +25°; in cases of strong coupling, the δs are according to first-order rules; signs of Js undetermined but assumed to behave according to well-known literature data): 4.65 (all acidic H + HDO); 4.25 (*dq*, J = 4.0, 6.4, H–C(2)); 4.09 (*d*, J = 4.0, H–C(3)); 4.05 (*d*, J = –18.2, H^R– or H^S–C(13)); 4.01 (*d*, J = –18.2, H^S– or H^R–C(13)); 3.57 (*s*, Me(11)); 3.45 (*s*, H^R–C(12), H^S–C(12)); 2.79 (*d*, J = –17.7, H^S–C(10)); 2.72 (*d*, J = –17.5, H^R–C(8)); 2.65 (*d*, J = –17.5, H^S–C(8)); 2.64 (*d*, J = –17.7, H^R–C(10)); 1.13 (*d*, J = 6.4, Me(1)). ^{13}C-NMR (D_2O, +25°): δ 172.24 (C(4)); 171.62 (C(14)); 158.81 (C(7)); 157.35 (C(5)); 123.73 (C(6));

68.90 (C(9)); 65.77 (C(2)); 65.25 (C(12)); 61.40 (C(3)); 57.28 (C(11)); 43.71 (C(13)); 31.10 (C(10)); 30.69 (C(8)); 17.11 (C(1)).

3. Ab initio *NMR Shift Calculations.* Quantum-chemical methods: All structures were fully optimized at the B3LYP/6-31G(d) density-functional-theory (DFT) level [22] by using the Gaussian 03 program [23]. Frequencies were computed at the same level to characterize stationary points and to obtain zero-point vibrational energies (*ZPE*s). All frequencies are unscaled. DFT, in particular B3LYP, was shown to provide accurate geometries and good harmonic vibrational frequencies for a broad range of molecules and ions (see, *e.g.*, [24]). As shown recently, the level of theory selected (B3LYP/6-31G(d)) is well suited for NMR [25][26] and NICS calculations [27]. Following the approach of *van Eikema Hommes* and *Clark* [26a], we converted the calculated magnetic shielding constants (σ) into δ(C) relative to $SiMe_4$ by applying *Eqn. 1* [26a].

$$\delta = 200.65 + (-1.0715\ \sigma)\ (R^2 = 0.9984) \quad (1)$$

4. *NMR-Shift Prediction.* ^{13}C-NMR-Shift predictions were carried out by using the online version of the software package 'NMRPredict' [28] on a *Microsoft-Windows-XP®*-based computer. 'NMRPredict' has been developed by Prof. *W. Robien* (Vienna) and Prof. *R. Abraham* (Liverpool). Different combinations of options were employed: Default solvent, default solvent + charged, solvents off and charged on, all H_2O solvents and charged on. No configurational information was provided in the input. Neural network and/or HOSE-code-based results were employed for comparison with measured data of **1**.

Results and Discussion. – 1. *Experimental NMR Spectra Including Scalar Coupling.* Both the ^{1}H- and the ^{13}C-NMR spectrum of **1** reveal the presence of only a single isomer. For convenience, we use the numbering shown in Formula **1**[1]). As usual under the employed measurement conditions, there is a rapid exchange of all acidic protons of compound **1** as well as of H_2O, HDO, and D_2O from the solvent. Accordingly, a single intense common signal is found at δ 4.65 in the ^{1}H-NMR spectrum. The assignment of the J(H,H) network of the threonine-derived residue in **1** (positions 1, 2, and 3) is derived straightforwardly from the COSY plot (*Fig. 1*,*a*).

The *d* at δ 1.13 (Me(1)) shows a cross-peak to the *dq* at δ 4.25 which must therefore be the signal of H–C(2). The latter in turn shares a cross-peak with the *d* at δ 4.09 (H–C(3)). Likewise, the protons of the MeO group (Me(11)) can be easily assigned to the *s* at δ 3.57.

There are a total of four CH_2 groups in the molecule, *i.e.*, CH_2(8), CH_2(10), CH_2(12), and CH_2(13). Due to the chirality of the molecule, the protons within each CH_2 group are diastereotopic. Their correct ^{1}H-NMR assignment (*Fig. 1*,*a*–*c*) is less trivial and is possible only by means of the HMBC and the NOE experiments (see below).

At the measurement frequency (500 MHz), the chemical-shift difference of H^R– and H^S–C(12)[1]) is minute, hence they appear pseudo-isochronously as a *s* at δ 3.45. In addition, a very small geminal coupling constant (*ca.* 1–2 Hz) between these protons can be expected anyway due to the attached O-atom (substituent effect on geminal coupling constants). H^R– and H^S–C(13) exhibit a larger chemical-shift difference and appear as a typical *AB* pattern at δ 4.01 and 4.05. Their assignment is shown in *Fig. 1*,*b*, however, with no further distinction between H^R– and H^S–C(13). A more complex situation is found for the proton pairs $H^{R/S}$–C(8) and $H^{R/S}$–C(10). However, from the COSY plot (*Fig. 1*,*c*), the coupling pattern may be derived unequivocally. Any residual

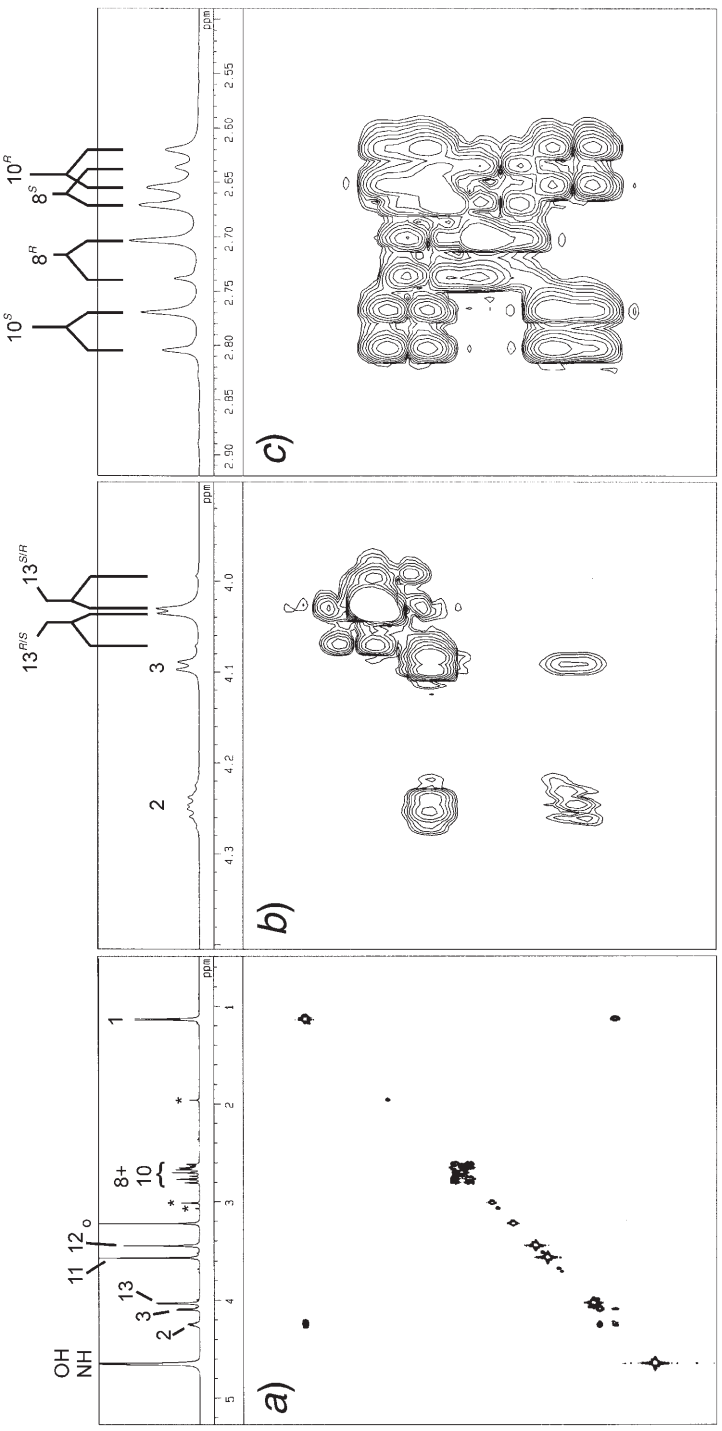

Fig. 1. *COSY Plot of* **1** *in* D_2O *solution*[1]) (*ca.* 0.01M, +25°; for spectral parameters, see *Exper.* a) *Full spectral width* (assignments refer to the atom numbering in *Formula* **1**[1]); o = residual MeOH (from the extraction procedure); * = other minor impurities). b) *Zoomed region of the resonances of H–C(2), H–C(3), and* $H^{R/S}$*–C(13)* (notice the coupling pattern of the diastereotopic $H^{R/S}$–C(13)). c) *Zoomed Region of the resonances* H^R*– and* H^S*–C(8) and* H^R*– and* H^S*–C(10)* (notice the coupling pattern of the diastereotopic $H^{R/S}$–C(8) and $H^{R/S}$–C(10)

ambiguities in the assignment of the proton resonances may be resolved by means of the HMBC experiment (see below).

Of the CH_2 resonance lines, the $CH_2(13)$ signals are shifted downfield due to the combined effects of the attached N-atom and the COOH group (δ 4.01 and 4.05, resp.). The $CH_2(12)$ signals appear at an 'expected' chemical shift (δ 3.45). The chemical shifts of $CH_2(8)$ (δ 2.65 and 2.72) and $CH_2(10)$ (δ 2.64 and 2.79) are influenced by the attached C=C and C=N bonds. Further configuration assignments of the prochiral-proton pairs are given below.

The correlations based on ^1J(H,C) couplings can be extracted from the HMQC plot shown in *Fig. 2* (HMQC = hetero multiple-quantum coherence). From the cross-peak pattern therein, unequivocal assignments of C-atoms which have attached protons may be derived. Thus, the δ(H) of the diastereotopic proton pairs $CH_2(8)$, and $CH_2(10)$ share the expected cross-peaks with the relevant δ(C).

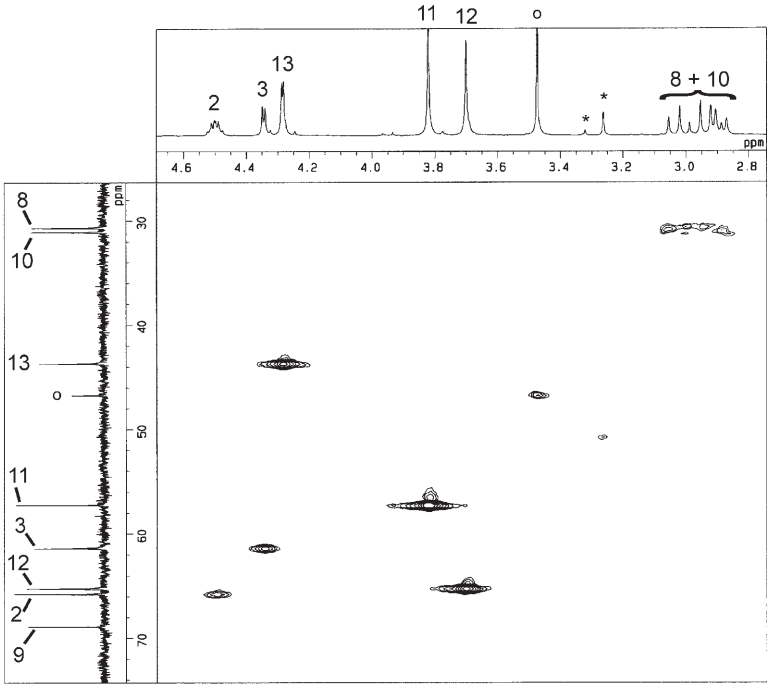

Fig. 2. *HMQC Plot of* **1** *in* D_2O *solution* (*ca.* 0.01M, +25°). Assignments refer to the atom numbering in *Formula* **1**. Cross-peaks indicate direct ^1J(H,C) couplings. For spectral parameters, see *Exper.* The δ(H) and δ(C) of Me(1) trivial assignments, (*i.e.*, threonine Me) are omitted; o = residual MeOH (from the extraction procedure); * = other minor impurities

The HMBC plot (HMBC = hetero multiple bond coherence) of *Fig. 3* is of special value for the assignment of the quaternary C-atom resonance lines which usually are the most demanding ones in NMR analyses. The cross-peak pattern shown *Fig. 3*, *a* thus unequivocally allows these C resonances to be assigned.

Not all cross-peaks in *Fig. 3* which are largely self-explanatory shall be discussed. Noteworthy, however, are the signals shown in *Fig. 3,b* and *c*. A cross-peak is found between the $CH_2(13)$ δ(H) and δ(C) 158.81, due to a ^3J coupling, which thus allows to unequivocally assign C(7) to the latter signal. In addition, a cross-peak between the δ(H) of $CH_2(13)$ and δ(C) 171.62 is due to a ^2J coupling between $CH_2(13)$ and C(14), and the cross-peaks within the box of *Fig. 3,b* are indicative of a ^2J coupling between H–C(3) and C(4).

2. *Nuclear*-Overhauser-*Effect* (NOE) *Measurements.* The measurements of NOEs of porphyra-334 (**1**), a powerful tool in structural analysis [19], were performed by both 1D and 2D NOE methods. Among the 1D NOE methods, the pulsed-field-gradient pulse sequence DPFGSE-NOE [18] has turned out to be the method of choice in recent years and has largely superseded conventional NOE difference spectroscopy (DPFGSE = double-pulsed-field-gradient spin echo). *Fig. 4* shows selected DPFGSE-NOE plots of **1**. Irradiation of the H–C(3) signal (*Fig. 4,b*) leads to the expected NOEs at the signals of Me(1) and H–C(2). In addition, and importantly, a strong NOE involving $CH_2(10)$ is found. No NOE is observed for the MeO group. This is an unequivocal evidence for the threonine-derived residue being in a configuration having H–C(3) in proximity to $CH_2(10)$, *i.e.*, *the configuration at the C=N bond must be (*E*)* (see *Formula* **1**). *Fig. 4,b* (inset), shows in addition that H–C(3) is in somewhat closer contact to H^R–C(10) as compared to H^S–C(10), thus giving even further insight into the preferred conformation of **1** in solution.

Irradiation at the MeO resonance line (*Fig. 4,c*) shows exclusively a very weak NOE to the Me(1) signal, in agreement with a conformation which positions the two Me groups approximately 5 Å apart. The diastereotopic protons H^S–C(12) and H^R–C(12) are accidentally isochronous (δ 3.45). When the corresponding *s* is irradiated (*Fig. 4,d*), strong NOEs appear at *two* of the four δ of $CH_2(8)$ and $CH_2(10)$. Hence, these protons must be the ones '*cis*' to the CH_2OH group and are thus attributed to H^R–C(8) and H^S–C(10). The corresponding NOEs which involve H^S–C(8) and H^R–C(10) are significantly weaker (inset of *Fig. 4,d*).

When the H–C(2) signal is irradiated (not shown), NOEs are found which involve exclusively Me(1) and H–C(3). Not even a weak NOE is detected for $CH_2(10)$ and $CH_2(12)$. Consequently, **1** must adopt a preferred conformation where H–C(2) points 'outward'. Irradiation of the signal of Me(1) (not shown) exhibits, apart from the expected NOEs at the δ of H–C(2) and H–C(3), a weak NOE at the signals of $CH_2(12)$ and at that of H^S–C(10). This is evidence for Me(1), H^S–C(10), and $CH_2(12)$ being in a '*cis*'-like conformational arrangement, in agreement with an absolute configuration (*S*) at C(9) (see below). When the resonance lines of the diastereotopic $CH_2(13)$ are irradiated (not shown), strong NOEs of approximately equal intensity are found for H^R–C(8) and H^S–C(8). This agrees well with the *ab initio* calculated preferred conformation of **1** and of its protonated form **6**, respectively (see below).

A 2D NOESY experiment of **1** nicely confirms the results obtained from the 1D DPFGSE-NOE experiment. *Fig. 5* shows selected zoomed areas of the contour plot. In *Fig. 5,a*, intense cross-peaks are found between the signals of H–C(3) and H^R–C(10), and a weaker cross-peak between those of H–C(3) and H^S–C(10). First, this is an unequivocal evidence for the threonine-derived residue being located as depicted in Formula **1**, *i.e.*, with (*E*)-configuration of the C=N bond. Second, we conclude that

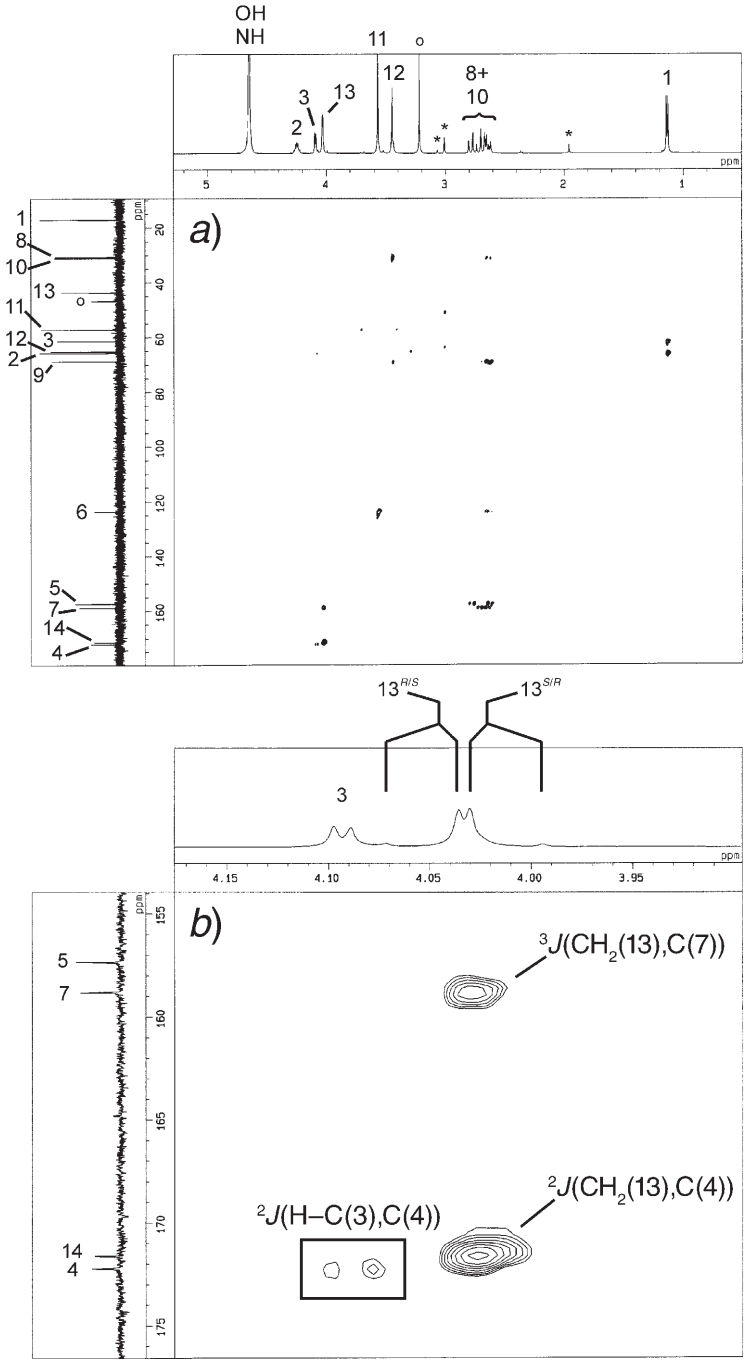

Fig. 3. *HMBC Plot of* **1** *in* D_2O *solution*[1]) (*ca.* 0.01M, +25°; cross-peaks indicate long-range ^2J(H,C) and ^3J(H,C); assignments refer to the atom numbering in *Formula* **1**). a) *Full spectral width* (o = residual MeOH (from the extraction procedure); * = other minor impurities. b) *Zoomed region of the resonances of H–C(3), CH_2(13), C(4), C(5), C(7), and C(14)* (the assigned cross peaks identify the relevant δ(C)). c) *Zoomed region of the resonances of CH_2(8), CH_2(10), C(5), and C(7)* (the assigned cross-peaks identify the relevant δ(C)).

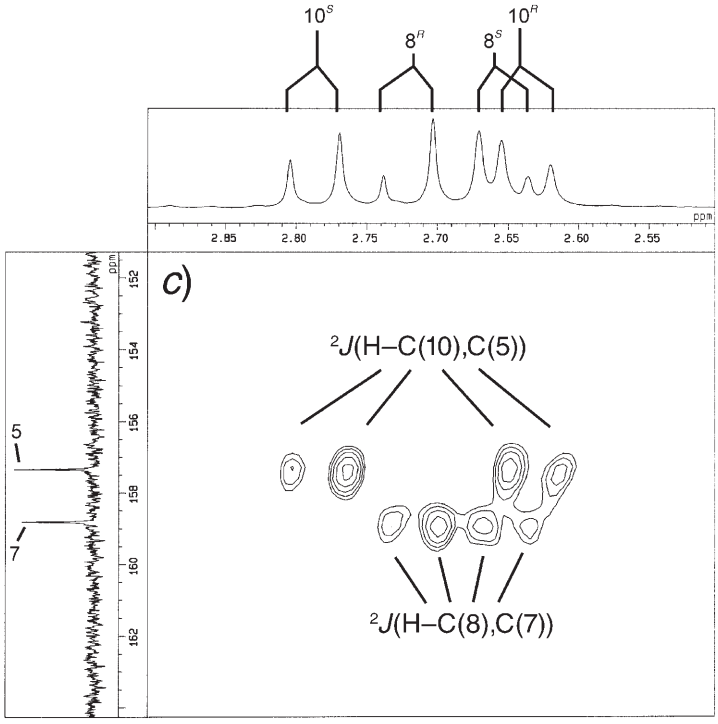

Fig. 3 (cont.)

H–C(3) is oriented preferably at the '*endo*' face, *i.e.*, in closer proximity to H^R–C(10) than to H^S–C(10). *Fig. 5*, *b*, represents the cross-peaks between CH_2(12) and CH_2(8) and CH_2(10). As in the DPFGSE-NOE experiment, the strong cross-peaks assign those protons which are closer to CH_2(12), *i.e.*, H^R–C(8) and H^S–C(10).

3. *Diffusion Measurements and Molecular Size.* We were additionally interested to investigate whether porphyra-334 (**1**) exists as a monomeric entity in H_2O solution or whether the molecule is aggregated in whatever state. A very convenient way for the determination of particle sizes by NMR has become popular in recent years. The diffusion constants of molecules may be measured by the application of pulsed-field gradients in combination with a suitable spin-echo sequence. The most intuitive way of presenting these results is DOSY (diffusion-ordered spectroscopy) [20] where a pseudo 2D plot permits the direct extraction of diffusion constants. However, the relevant values may also be obtained in a more classical approach by means of the *Stejskal–Tanner* method [21]. Here, with a suitable pulse sequence, a series of spectra is recorded with incremental increase of the gradient strengths applied during the pulse sequence. The decay of the signal intensities during this series is a direct measure for the involved diffusion constants which, in turn, may be used to extract the hydrodynamic radii of the involved molecules from the *Stokes–Einstein* equation. The relevant relations are given by *Eqns. 2* and *3*. Therein, D is the diffusion constant, k the *Boltzmann*'s constant, T the absolute temperature, η the solvent viscosity, r_H the

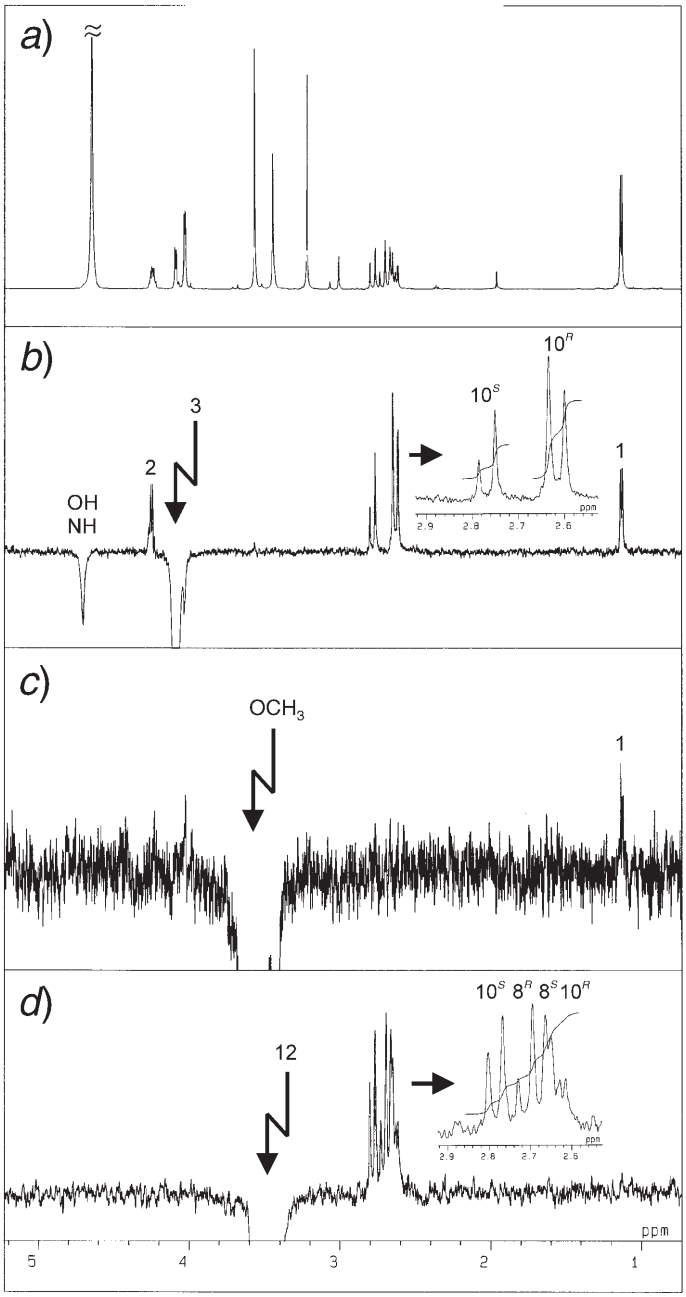

Fig. 4. *1D NOE Plots* (DPFGSE sequence) *of porphyra-334* (**1**) *in* D_2O *at* $+25°$[1]) (for atom numbering, see *Formula* **1**). a) *Normal* ^{1}*H-NMR spectrum*. b) *Irradiation at H–C(3)* (intense direct (pos.) NOEs for H–(2) and Me(1), indirect (neg.) NOE at the HDO signal; intense pos. NOE for H^R–C(10) and a weaker pos. NOE for H^S–C(10)). c) *Irradiation at Me(11)O* (only very weak NOE for Me(1), no further NOEs, establishing the (*E*)-configuration at C=N). d) *Irradiation at* CH_2*(12)* (intense NOEs for H^R–C(8) and H^S–C(10); weaker NOEs for H^S–C(8) and H^R–C(10)).

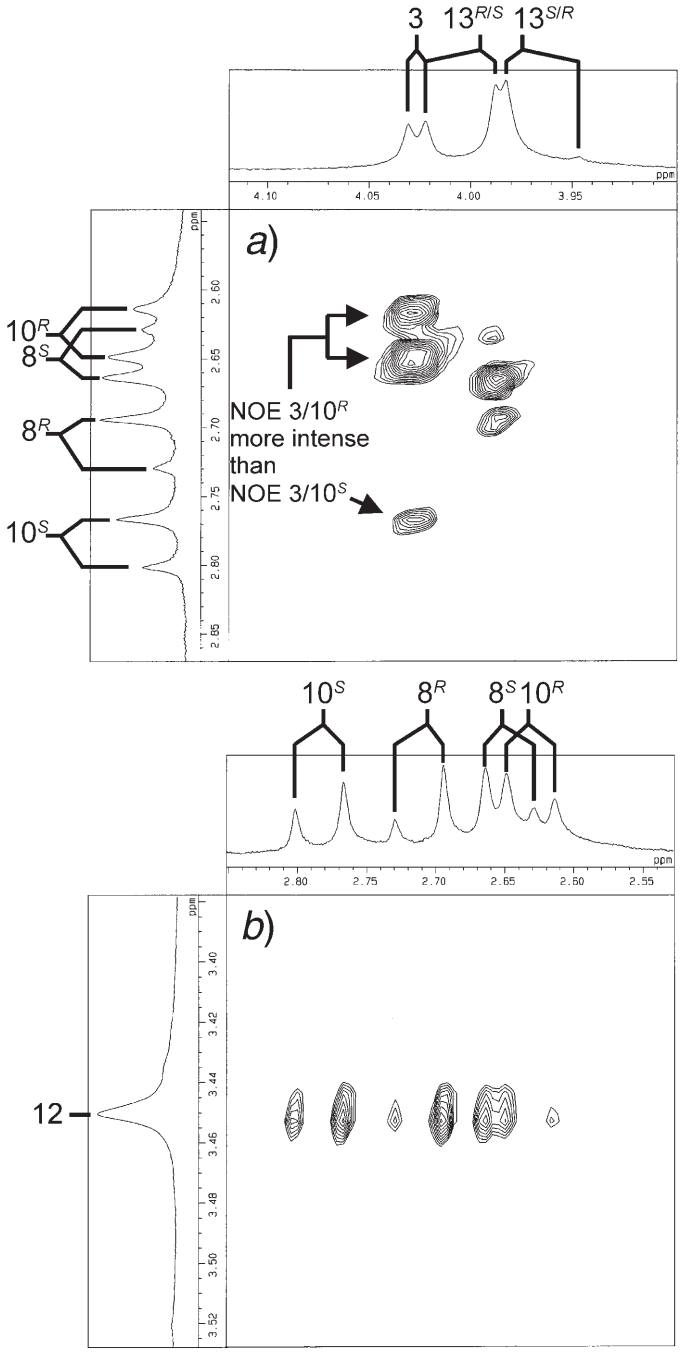

Fig. 5. *Phase-sensitive NOESY experiment with porphyra-334* (**1**) *in* D_2O *at* $+25°$[1]) (for atom numbering, see *Formula* **1**). a) *Zoomed region of cross-peaks between H–C(3) and* CH_2*(13), and* CH_2*(8) and* CH_2*(10)* (intense cross-peaks between H–C(3) and H^R–C(10) indicate close proximity, as well as close proximity between CH_2(13) and CH_2(8)). b) *Zoomed region of cross-peaks between* CH_2*(12), and* CH_2*(8) and* CH_2*(10)* (more intense cross-peaks for H^R–C(8) and H^S–C(10) which are *cis* to CH_2(12) as compared to those for H^S–C(8) and H^R–C(10) which are *trans* to CH_2(12)).

hydrodynamic radius, I the signal intensity in the presence of the applied gradient, I_0 the signal intensity without gradient, γ the magnetogyric ratio of ^{1}H, G the gradient strength, δ the gradient duration, and Δ the diffusion delay.

$$\textit{Stokes}-\textit{Einstein}\text{ equation: } D = kT/(6\pi\eta r_H) \quad (2)$$

$$\textit{Stejskal}-\textit{Tanner}\text{ equation: } \ln(I/I_0) = \gamma^2 G^2 \delta^2 (\Delta - \delta/3) D \quad (3)$$

A series of ^{1}H-NMR spectra was recorded by using the BPP-LED (bipolar pulse pair longitudinal eddy current delay) pulse sequence [20]. During the sequence of the 32 individual spectra, the gradient strength was increased up to 0.9 T/m. The signal intensity of the threonine-derived Me(1) group in prophyra-334 (**1**) was taken as an indicator, and the signal intensities (as $\ln(I/I_0)$) are plotted in *Fig. 6* against G^2. The slope of the least-squares-fit line is indicative of the diffusion constant D of **1**. As an internal reference, the signal of monodeuterated water (HDO) was employed. As expected, water diffuses considerably faster than **1**, resulting in a faster decay of the water resonance lines during the measuring sequence and, hence, a larger slope for the water-derived line in *Fig. 6*.

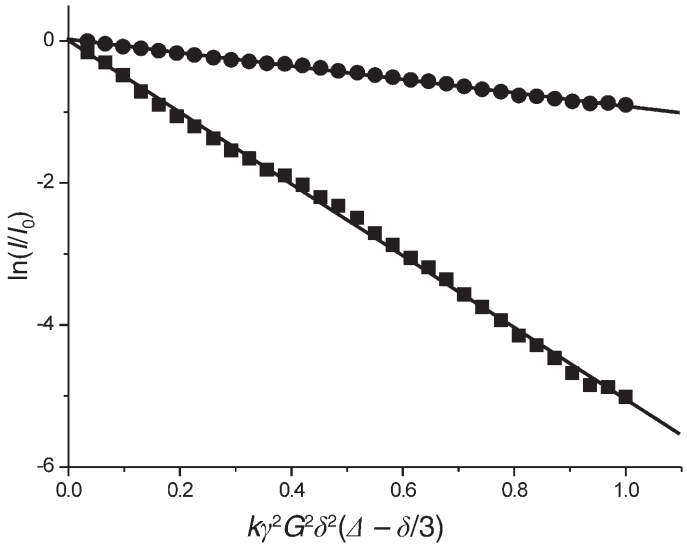

Fig. 6. *Pulsed-gradient spin echo* (PGSE) *measurements on porphyra-334* (**1**) (*Stejskal–Tanner* plot) *at 30°*. ■ = water signal (HDO); ● = signal of the threonine Me(1) group of **1**, k = scaling factor, γ = magnetogyric ratio of ^{1}H, G = gradient strength, δ = gradient duration (1 ms), Δ = diffusion delay (50 ms). A series of 32 individual spectra was recorded with increasing gradient strengths G; maximum gradient strength = 0.9 T/m. The solid lines are least-squares fits to the data. The slope of the curves represents the diffusion constant according to the *Stejskal–Tanner* equation [21]. The slope of the HDO signal was taken as an internal reference according to the hydrodynamic radius of H_2O (= 0.765 Å) (*via* the *Stokes–Einstein* equation). This yields a hydrodynamic radius of 4.39 Å for **1**.

By comparison of the slopes in *Fig. 6* for **1** and for water, by using a hydrodynamic radius $r_H = 0.765$ Å for water, and by using the *Stokes–Einstein* equation (*Eqn. 2*), we

obtained a hydrodynamic radius of porphyra-334 (**1**) of 4.39 Å. This agrees very well with a molecule radius derived from molecular models and from the calculations (see below) of *ca.* 4.5 Å. Thus, in water solution **1** is *strictly monomeric*, no aggregation can be detected by the diffusion measurements.

4. Ab initio *^{13}C-NMR Chemical Shift Calculations.* The data obtained by our NMR studies do *per se* not allow an unambiguous determination whether **1** is present in its neutral form, in one of its mono-betaine structure **2** and **3**, or in its bis-betaine structure **4**. Furthermore, as the extraction procedure of porphyra-334 (**1**) included contact with HCl, the monoprotonated species **5** and **6** might be present in solution, as well as a bis-protonated species **7**. A distinction of the different species **1**–**7** should be made possible by comparing the experimental ^{13}C-NMR chemical shifts with those obtained by *ab initio* calculations or those obtained by suitable prediction software. Moreover, *ab initio* calculations might reveal the presence of intramolecular H-bonds. For convenience and for simplification, we neglected the indication of the configurations at the stereogenic centers in *Formulas* **2**–**7**. However, all our *ab initio* calculations included the correct configurations, *i.e.*, those shown in *Formula* **1**.

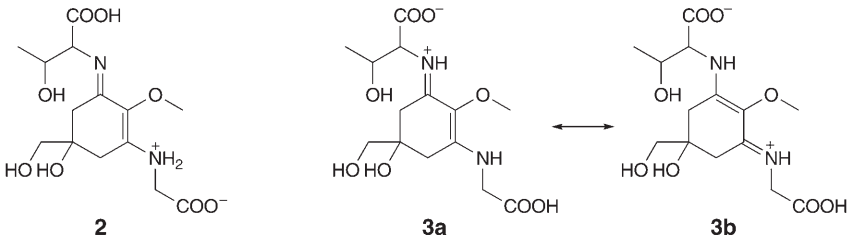

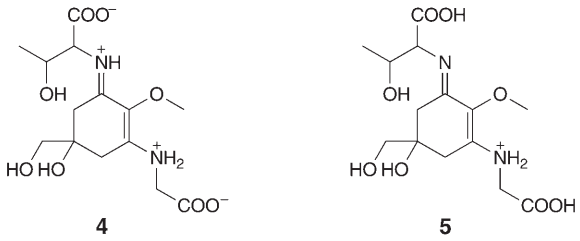

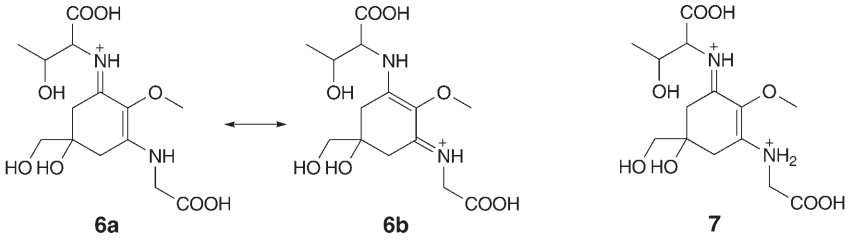

With respect to the chosen level of calculation, a recent paper [26a] claims: 'There is little to choose between the two levels of calculation (B3LYP/6-31G(d) and B3LYP/6-

311 + G(d,p)) and, perhaps surprisingly, the extra polarization functions on hydrogen do not improve the performance for ^{1}H chemical shifts. Thus, we can conclude that B3LYP/6-31G(d)//B3LYP/6-31G(d) is an adequate level for calculating chemical shifts for both ^{13}C and ^{1}H economically and reliably.' We thus employed the B3LYP/6-31G(d) theory level for our calculations exclusively.

The *ab initio* calculated δ(C)s for structures **1**, **3** and **5**–**7** are given in *Table 1*. Various isomers with intramolecular H-bonds were also calculated. Strikingly, the best fit with the experimental data is found for those isomers where the imino N-atom is protonated and the glycine N-atom is formally neutral, *i.e.*, structures **3** and **6**. This fits nicely the results obtained with the 'NMRPredict' software package (see below, *Sect. 7*). The *ab initio* calculated structure **6** which we believe to be prevailing in D_2O solution is depicted in *Fig. 7*, along with indicated H-bonds.

5. Ab initio *Calculated Stabilities, Proton Affinities, and the Porphyra-334 'Proton Sponge'*. The relative stabilities of the calculated structures are shown in *Table 2*. Structures **2** and **4** were not subsumable by our gas-phase *ab initio* calculations since the proton of the $R_2NH_2^+$ group migrated back to the COO^- group in all attempts. This behavior is not uncommon and well documented for calculations of zwitterionic systems like amino acids or their derivatives [29a]. The most satisfying prevention

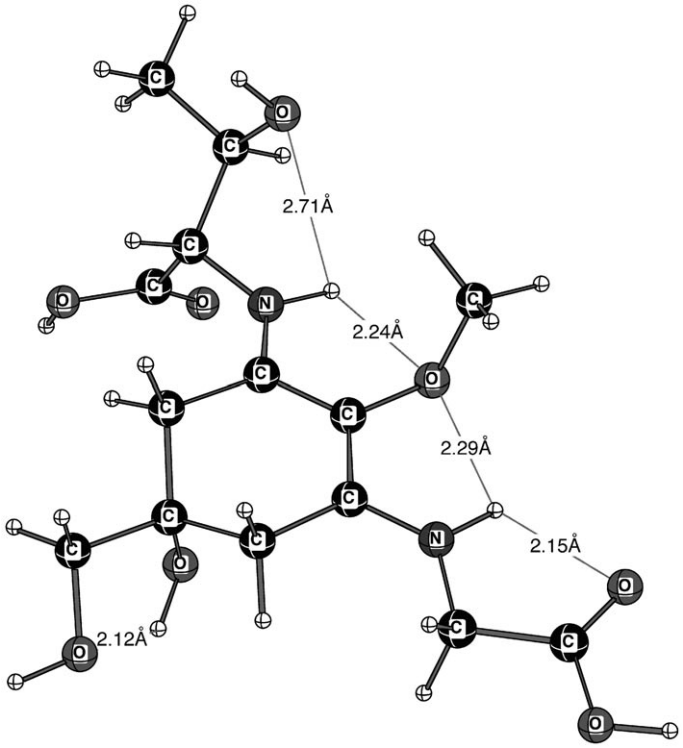

Fig. 7. *DFT-Calculated structure of* **6**, *the imino N-atom protonated form of* **1**. Note the indicated H-bonds.

Table 1. *^{13}C-NMR Chemical Shifts* [ppm] *of* **1**, **3**, *and* **5**–**7** *as Calculated by the DFT Methods.* In addition, some structures were calculated by including H-bonds as described in the *Footnotes a–e.* Structures **2** and **4** are omitted from *Table 1* since glycine in its betaine form is not stable in the gas phase. For statistical significance of the data, see [26a].

C	**1**	**1**[a])	**1**[b])	**3**	**3**[c])	**3**[d])	**5**	**6**[e])	**7**	Exper. δ(C)
C(1)	23.50	17.81	23.32	25.13	20.52	21.23	18.47	18.98	17.63	17.11
C(2)	69.85	72.02	69.80	70.51	73.02	70.77	71.34	72.67	77.03	65.77
C(3)	72.55	68.33	72.34	76.38	69.99	74.38	74.05	65.82	74.35	61.40
C(4)	172.89	179.60	172.67	154.41	159.47	161.82	169.80	167.13	164.71	172.24
C(5)	161.44	164.40	162.98	162.98	168.07	176.61	159.99	160.78	183.44	157.35
C(6)	135.40	134.07	130.20	128.06	127.06	125.37	154.40	126.82	147.72	123.73
C(7)	141.89	142.74	139.16	150.25	153.45	147.68	119.68	161.37	147.77	158.81
C(8)	33.10	34.81	40.16	34.42	43.53	43.01	34.77	36.46	35.25	30.69
C(9)	71.54	72.72	71.77	71.35	78.92	74.59	76.62	76.31	81.39	68.90
C(10)	38.70	38.09	38.53	36.96	38.92	39.44	43.28	34.46	42.54	31.10
C(11)	56.39	57.73	57.30	57.18	56.57	61.64	64.44	57.94	65.48	57.28
C(12)	73.48	73.41	72.78	72.23	69.55	72.19	69.44	71.04	68.86	65.25
C(13)	46.81	46.69	51.08	45.46	48.79	51.04	57.18	43.56	51.47	43.71
C(14)	166.60	166.28	165.05	163.94	163.27	161.84	157.37	165.91	162.42	171.62

[a]) H-Bridge from glycine N*H* to glycine CO*O*H; H-bridge from threonine O*H* to threonine C*O*OH. [b]) H-Bridge from glycine COO*H* to Me*O*. [c]) H-Bridge from glycine COO*H* to *O*H–C(9); H-bridge from threonine O*H* to COO^-; H-bridge from threonine N*H* to Me*O*. [d]) H-Bridge from glycine COO*H* to Me*O*; H-bridge from threonine N*H* to Me*O*; H-bridge from threonine O*H* to COO^-. [e]) H-Bridges as depicted in *Fig. 7*.

against proton back-migration would be the inclusion of solvent water molecules [29b]. However, since **6** is the most probable species present (supported by good agreement between experimental and calculated δ(C)s; see above, *Sect. 4*), we have not added water molecules.

Table 2. *Calculated Relative Stabilities* (RB3LYP/6-31G(d)) *of Neutral and Protonated Isomers of Porphyra-334* (**1**)

	1	**2**	**3**	**4**	**5**	**6**
Relative stability [kcal/mol]	0	–	6.0[a])	–	42.4[b])	0

[a]) Relative to **1**. [b]) Relative to **6**.

There is a second common and well documented problem in studying zwitterionic systems with quantum-chemical methods: Zwitterionic isomers are usually higher in energy than the corresponding nonzwitterionic systems [30]. In our case, **3** is calculated to be 6.0 kcal/mol less stable than **1**.

The nonzwitterionic species **1** shows exemplarily for all isomers and protonated species that within the investigated molecules, no strong H-bonds are possible. Instead, one can find a couple of weak interactions between NH or OH groups and O-atoms. In **1**, there are two weak interactions between the NH group of the glycine side chain and

the glycine OH (2.25 Å) and the MeO group (2.17 Å). A contact is also observed between the O*H*–C(9) and the *O*H–C(12) (2.13 Å).

Protonation of nonzwitterionic **1** leads to **5** or **6**, respectively. Of these species, **6** is clearly favored as compared to **5** by more than 42 kcal/mol. Interestingly, the protonated imino group has a stabilizing effect on the conformation of the threonine-derived chain with weak NH–O interactions of 2.15, 2.29, 2.24, and 2.19 Å, respectively (see *Fig. 7*). This nicely reflects the conformation of porphyra-334 (**1**) found experimentally by the NOE experiments (see above), *i.e.*, H–C(3) is close to H^R–C(10) and H^S–C(10), whereas H–C(2) points 'outward' and is remote from the ring moiety.

The calculated gas-phase proton affinity of **1** is 265.7 kcal/mol (*Table 3*). This number is in the range of the gas-phase proton affinity of super bases [31] like the so-called 'proton sponge' *N*,*N*,*N*′,*N*′-tetramethylnaphthalene-1,8-diamine (**8**) [32], the well known cryptand 1,6-diazabicyclo[4.4.4]tetradecane (**9**), cryptand **10** (also termed '[1.1.1]'), cryptand **11** (also termed '[2.2.2]') [33], and hexaethylenetetramine **12** [34]. *Thus, porphyra-334* (**1**) *behaves as a 'proton sponge' with a proton-capturing power comparable to other synthetic systems studied so far. To the best of our knowledge,* **1** *thus represents the first described 'natural' proton sponge.* Whereas the high electron density of close-by basic centers is responsible for the exceptional proton affinity of the proton sponge **8** and of the cryptands **9**–**12**, we attribute the extraordinary high proton affinity of **1** to a completely different origin. After protonation of **1**, the two N-atoms in **6** are very akin to similar neighboring groups connected by three sp^2 C-atoms. Therefore, the positive charge can be delocalized between the two N-atoms and the C_3-moiety (N–C(5)–C(6)–C(7)–N). This push–pull type of stabilization was proposed by *Schwesinger* [35] for 2,3,5,6,8,9-hexahydro-1*H*-diimidazo[1,2-*d*:2′,1′-*g*][1,4]diazepine (**13**) and related nonionic superbases like **14**, with **14** being a system which additionally consists of close-by basic centers. Actually, **13** represents best the electronic situation found in porphyra-334 (**1**). Since in **5** no delocalization of the charge is possible, this mechanism also explains the large stability difference between the isomers **5** and **6**.

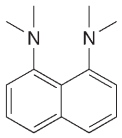

8

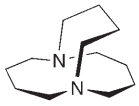

9

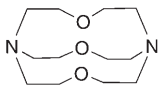

10

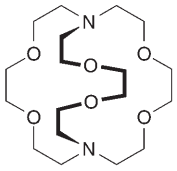

11

12

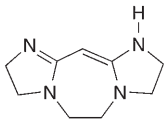

13

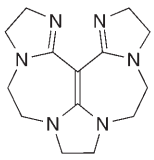

14

Table 3. *Experimental and Calculated* (RB3LYP/6-31G*) *Proton Affinities* (increasing numbers from top to bottom) *of* **1** *and Other Bases.*

	Proton affinity [kcal/mol] (exper.) [36]	Proton affinity [kcal/mol] (RB3LYP/6-31G*)
NH_3	– 202.3	– 207.5
Pyridine	– 219.9	– 224.5
Me_3N	– 224.8	– 226.5
8	– 241.5	– 242.5
11	–	– 253.1
10	–	– 253.3
12	–	– 256.4
15	–	– 261.1
9	–	– 261.3
1	–	– **265.7**
13	–	– 266.9
14	–	– 279.6

We attribute this postulated origin of the 'proton-sponge' effect of **1** also to another observation: whereas, *e.g.*, in 'hexaethylenetetramine' **12**, a 'captured' proton is 'fixed' and even exhibits scalar coupling to the 'surrounding' protons [34b], no such effect is observed for **1**. All 'acidic' protons still undergo rapid exchange on the NMR time scale.

The high proton affinity of porphyra-334 (**1**) found by our calculations nicely correlates with experimental studies by *Ogawa* and co-workers [37]. It has been found by using UV spectroscopy that **1** is stable in the pH range from 1 to 11. However, depending on temperature, in more basic media ($\geq$ pH 12), **1** decomposes more or less rapidly. This behavior might be of interest with respect to commercial applications of **1**, *e.g.*, in sunscreens (contact with alkaline soap solutions). To the best of our knowledge, the nature of the decomposition products of **1**, as well as the decomposition mechanisms, are unknown. Possibly, the imino group of **1** or the imino-analogue *Michael* system, respectively, are less prone to nucleophilic attack when porphyra-334 is protonated.

6. *Rotational Barrier of the Protonated Imino Group in Porphyra-334* (**1**). In neutral **1**, the (*E*)-configuration at the imino group can be expected to be stable. However, the *ab initio* calculations as well as the ^{13}C-NMR data from 'NMRPredict' suggest that under our experimental conditions, we observe the imino-protonated species **6**. Hence, the question arises whether also the protonated imino group in **1** is configurationally stable (*i.e.*, high barrier to rotation for (*E*)/(*Z*) isomerization), and whether the configuration (*E*) is thermodynamically more stable than (*Z*).

We chose model compound **15** for our calculational studies. *Fig. 8* shows the transition from the (*E*,*E*) ground-state across the transition state (*E*,TS) (where the substituents at the protonated imino group are perpendicular to the ring plane) to the ground-state (*E*,*Z*). The (*E*,*Z*) configuration is less stable than (*E*,*E*) by 2.2 kcal/mol. By using the *Gibbs* equation ($\Delta G = -RT\ln K$), we calculate that at 298 K, there should be a 43 : 1 equilibrium in favor of the (*E*,*E*)-isomer of **15**. Thus, even if a rapid (*E*/*Z*)-isomerization of **6** would take place at room temperature, the (*Z*)-isomer would not be detectable by NMR and would not even manifest itself in the NOE spectra.

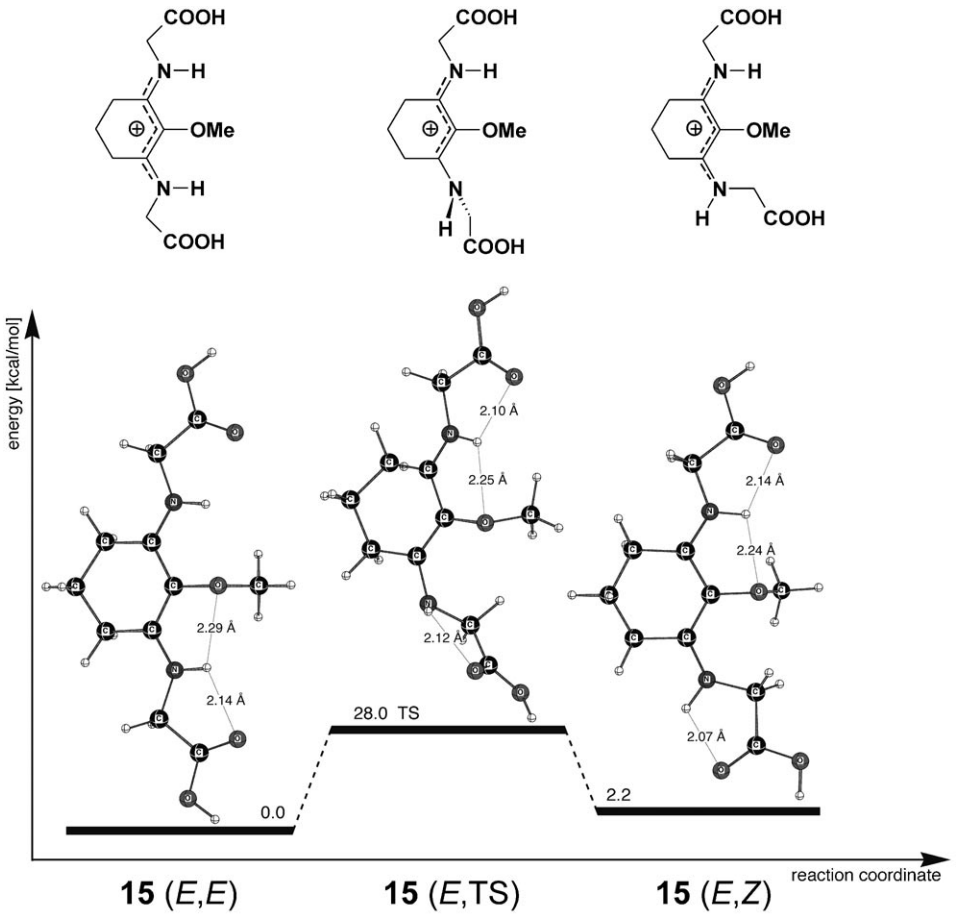

Fig. 8. *Calculated rotation in* **15** (taken as a model for the imino N-protonated species **6**) *around the formal C=N bond*. (*E*) and (*Z*) denote configurations according to the CIP rules; TS = transition state.

The rotational barrier of the protonated imino group in **15** (*Fig. 8*) is calculated to be 28.0 kcal/mol. This means that even after protonation of porphyra-334 (**1**), the conversion from (*E*) to (*Z*) at the imino group is an extremely slow process (from the *Eyring* equation: $k = 1.8 \cdot 10^{-8}\ s^{-1}$ at 298 K in model compound **15**). Hence, even in its protonated form **6**, porphyra-334 is configurationally stable at the imino group and is expected to retain the (*E*)-form. From the ^{1}H-NMR spectrum (*cf. Fig. 1,a*) it is evident that the exchange of acidic protons is a rapid process on the NMR time scale under our conditions.

7. *^{13}C-NMR Chemical Shifts from 'NMRPredict'*. A newly developed NMR prediction software package, 'NMRPredict' [28] is based on currently 345000 experimental structures. The ^{13}C-NMR chemical shift predictions are based both on the HOSE code algorithm as well as on a neural-network algorithm. We employed 'NMRPredict' to gain further insight into the correctness of our experimental δ(C)

assignments as well as to decide which of structures **1**–**7** is present in solution. For the predictions, the keywords 'default solvent', 'default solvent + charged', 'solvents off, charged on', and 'water solvents, charged on' were employed. The differences of the predicted shift values were relatively small. Thus, we present here only data obtained by using the keyword 'default solvent'. No configuration specifications of the stereogenic centers were given.

Table 4 shows the 'NMRPredict' chemical shifts δ(C) for structures **1**–**7**, along with the experimental values. Most important for the assignment of possible protonation sites are C(5), C(6), and C(7). Structures **1**, **2**, and **5** exhibit large deviations for carbon C(5) as compared to the measured value (δ 157.35). By contrast, structures **3**, **4**, **6**, and **7** show good agreement. We thus conclude that the prevailing species in solution must be protonated at the imino N-atom. Moreover, structures **3** and **6** also exhibit good agreement for the δ(C) of C(6). This indicates that the glycine-derived N-atom is *not* protonated under the experimental conditions, in agreement with the above stated reluctance of glycine to exist in the betaine form in the gas phase, as well as in agreement with the 'proton-sponge' arguments given above. Hence, 'NMRPredict' suggests that structures **3** and **6** are most likely to be prevailing under the experimental conditions. This agrees well with the *ab initio* calculations. A relatively large discrepancy between the predicted and the experimental δ(C) is found for C(7). We attribute this to the H-bonds described above for the DFT calculations and as depicted in *Fig. 7* which cannot be included into 'NMRPredict'.

Table 4. *^{13}C-NMR Chemical Shifts* [ppm] *of* **1**–**7** *as Predicted by the Software Package 'NMRPredict'*. The option 'default solvent' was selected. The δ(C) printed in italics for structures **3** and **6** are in good agreement with the experimental δ(C) for the involved C-atoms, whereas the corresponding C-atoms of other structures exhibit large deviations, indicating that the prevailing species in solution must be protonated at the imino N-atom.

	1	**2**	**3**	**4**	**5**	**6**	**7**	Exper. δ(C)
C(1)	21.1	21.1	20.4	20.4	21.1	20.4	20.4	17.11
C(2)	69.9	69.9	70.4	70.4	69.9	70.1	70.1	65.77
C(3)	73.8	73.8	64.4	64.4	73.8	64.4	64.4	61.40
C(4)	175.6	175.6	175.6	175.6	175.6	174.4	174.4	172.24
C(5)	171.7	173.6	*154.7*	154.7	173.6	*154.7*	154.7	157.35
C(6)	126.2	138.1	*125.9*	135.3	138.1	*125.9*	135.3	123.73
C(7)	145.4	150.0	142.9	150.0	150.0	142.9	150.0	158.81
C(8)	36.8	36.4	36.8	36.4	36.4	36.8	36.4	30.69
C(9)	69.5	69.8	69.4	69.8	69.8	69.4	69.8	68.90
C(10)	40.8	40.8	37.9	37.9	40.8	37.9	37.9	31.10
C(11)	60.9	60.9	60.9	60.9	60.9	60.9	60.9	57.28
C(12)	69.7	69.7	69.7	69.7	69.7	69.7	69.7	65.25
C(13)	50.5	48.8	50.5	48.8	49.3	50.5	49.3	43.71
C(14)	172.4	175.0	172.4	175.0	170.9	172.4	170.9	171.62

8. *Stereochemistry and Biochemistry.* From the biochemical synthesis of **1** it is evident that the side chain at the imino N-atom (C(1), C(2), C(3), and C(4) in *Formula* **1**) originates from L-threonine. Hence, we conclude that the configuration at the stereogenic centers C(2) and C(3) is as depicted, *i.e.*, (2*R*,3*S*). The third stereogenic

center in porphyra-334, C(9) in *Formula* **1**, is worth being analyzed in more detail. An 'ab initio' assignment of the configuration at C(9) by NMR is considered to be difficult without inclusion of the signals of the OH protons. Under our measurement conditions, there is rapid exchange of all acidic protons of **1** and of the water protons which appear as an averaged signal at δ 4.65 in the ^{1}H-NMR spectrum. Hence, this resonance line is not of diagnostic value.

However, there is strong biochemical evidence that mycosporin-glycine **16** is a precursor of porphyra-334 (**1**). It is widely agreed that **16** is biochemically derived from 3,3-*O*-didehydroquinic acid (**17**) [12][38]. Thus, during the biochemical transformations of **17** to **16**, two stereogenic centers get lost whereas the stereogenic center originally bearing the COOH group is retained, and the COOH group is subsequently reduced to yield the CH_2OH group in **16**. In very elaborate laboratory syntheses, *White et al.* [39] were able to establish that natural mycosporine-glycine **16** has the absolute configuration (*S*) as shown in *Formula* **16**. Based on these results, we conclude that the configuration (9*S*) is retained in the final porphyra-334 (**1**) and that the stereochemical relationships must be as depicted in *Formula* **1**. This is the basis of our assignments of the diastereotopic proton pairs $H^{R/S}$–C(8) and $H^{R/S}$–C(10) by NOE (see above, *Sect. 2*).

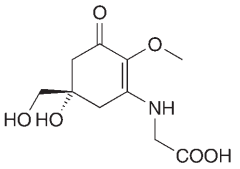

16

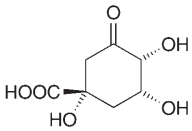

17

9. *Discussion of Literature Data.* An assignment for the ^{13}C-NMR spectrum of porphyra-334 had been given earlier by *Hirata* and co-workers in [2a]. The assignments of the proton-bearing C-atoms therein completely match our assignments given here. However, the authors of [2a] noted that their assignments of C(4)/C(14) and C(5)/C(7) are ambiguous and might as well be reversed. Our results, by means of the HMBC data of *Fig. 3*, actually establish that the assignments of [2a] for these C-atoms were incorrect and must be exchanged.

Slightly differing ^{13}C-NMR data for **1** were provided by the same authors in [2b], along with 270-MHz ^{1}H-NMR data for **1**. Therein, the diastereotopic nature of the ring protons CH_2(8) and CH_2(10) of **1** was realized, however, no assignments were given.

In a recent paper, *Srebnik* and co-workers [40] reported NMR studies on porphyra-334 (**1**). The ^{13}C-NMR data reported therein match our assignments with respect to the numerical sequence. In particular, the assignment of the quaternary C-atoms C(4)/C(14) and C(5)/C(7) is in agreement with our data. The ^{13}C-NMR chemical shifts given in [40] are generally *ca.* 1.5 ppm larger than our values. We attribute this to different referencing procedures (no referencing details for δ(C) are given in [40]). However, in some cases, there are even larger differences which may be due to different states of protonation of porphyra-334 (**1**) under the conditions used in [40] and under our conditions. The authors of [40] concluded that the structure should be represented as depicted in *Fig. 9*; however, we question whether this structure is correct. Rather, we

believe that our structure presented in *Formula* **1** meets the actual conditions. First, our NOE data unequivocally establish that the configuration at the C=N imino group *must be (*E*)* rather than (*Z*) as is shown in *Fig. 9* (*i.e.*, the threonine-derived side chain must be '*cis*' to the CH_2OH group). Next, the structure in *Fig. 9* shows, in our view, an incorrect configuration within the threonine-derived residue, *i.e.*, the C(α) atom is shown with configuration (*R*) and the C(β) atom with configuration (*S*). This assignment is opposite to the configurations found in naturally occurring L-threonine. Furthermore, the authors of [40] do not comment on the configuration at the stereogenic center C(9). Also, we do not understand why the glycine-derived residue in *Fig. 9* is drawn with a wedged bond, whereas in reality there is coplanarity with the conjugated C=C bond.

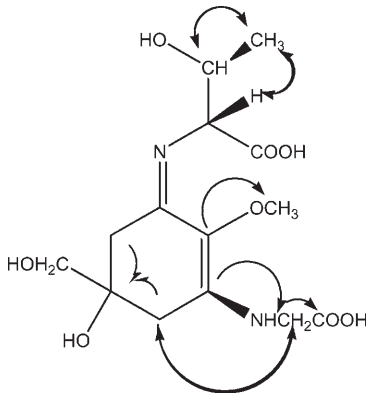

Fig. 9. *Facsimile of the proposed structure of porphyra-334 given in* [40]. For clarity and to avoid confusion with the numbering employed in this paper, the numbering in the formula was removed. Arrows in this reproduction are claimed by the authors to indicate multiple bond (HMBC; →) and NOE (↔) correlations. For a discussion questioning the correctness of this published structure, see text. Reproduced by permission of The Royal Society of Chemistry (RSC) on behalf of the European Society for Photobiology and the European Photochemistry Association.

In porphyra-334 (**1**), there are a total of four CH_2 groups. Due to the chirality of the molecule, each proton pair inherently consists of *diastereotopic* protons. In our spectra, this is clearly reflected in *Fig. 1*, *b* and *c*, for the proton pairs $H^{R/S}$–C(8), $H^{R/S}$–C(10), and $H^{R/S}$–C(13). By contrast, the authors of [40] report only *single* chemical shifts for these positions which is certainly an incorrect and misleading description.

Conclusions. – In this paper, a comprehensive analysis of the ^{1}H- and ^{13}C-NMR spectra of porphyra-334 (**1**) in D_2O is given. In addition, by using 1D- and 2D-NOE methods (DPFGSE-NOE, NOESY), we were able to assign prochiral pairs of protons at the ring positions. Diffusion measurements based on pulsed-field-gradient methods (PGSE, DOSY) confirmed that **1** is strictly monomeric in D_2O. By using DFT calculational methods, the ^{13}C-NMR chemical shifts of **1** were obtained. In addition, differently protonated forms of **1** were calculated (structures **2**–**7**). Best fits were obtained for those species which are protonated at the imino N-atom and which exhibit intramolecular H-bonds. From the *ab initio* calculations it became evident that **1** has an

exceptionally large proton affinity of 265.7 kcal/mol and behaves like a very powerful 'proton sponge', of comparable strength as synthetic systems studied so far. To the best of our knowledge, porphyra-334 (**1**) represents the first described 'proton sponge' of natural origin. This is due to the push–pull system in **6** which is formed after protonation of **1**. It remains to further investigations whether the high proton affinity of **1** is related to the effectiveness of **1** as a UV-absorbing component under environmental conditions. Furthermore, the stability of **1** in the pH range 1–11, as well as the rapid decomposition at pH > 12 is an indication that under 'natural' conditions, the imino-protonated species is present. The ^{13}C-NMR-DFT results are corroborated by ^{13}C-NMR chemical shift predictions obtained from the 'NMRPredict' software package. The absolute configuration (9*S*) of the stereogenic ring member C(9) of porphyra-334 (**1**) is derived from the absolute configuration (*S*) found in mycosporine-glycine **16** as well as from NOE experiments. Our NOE data contradict a structure of **1** recently proposed by *Srebnik* and co-workers [40]: clearly, the configuration at the imine moiety of **1** must be (*E*) rather than (*Z*).

We are grateful to the *Deutsche Forschungsgemeinschaft* (*DFG*) for financial support. Helpful discussions with respect to the 'NMRPredict' software package with Prof. *Wolfgang Robien* (Vienna) are gratefully acknowledged. We thank Prof. *Tim Clark* for hosting this work at the *CCC*, Dr. *Nico van Eikema Hommes* for helpful discussions, and the *Regionales Rechenzentrum Erlangen* (*RRZE*) for a generous allotment of computer time.

REFERENCES

[1] F. R. Abdulla, S. R. Feldman, P. M. Williford, D. Krowchuk, M. Kaur, *Pediat. Dermatol.* **2005**, *22*, 501.
[2] a) S. Takano, A. Nakanishi, D. Uemura, Y. Hirata, *Chem. Lett.* **1979**, *8*, 419; b) J. Kobayashi, H. Nakamura, Y. Hirata, *Tetrahedron Lett.* **1981**, *22*, 3001.
[3] K. Whitehead, J. I. Hedges, *J. Photochem. Photobiol., B* **2005**, *80*, 115.
[4] F. R. Conde, M. S. Churio, C. M. Previtali, *J. Photochem. Photobiol., B* **2000**, *56*, 139.
[5] F. R. Conde, M. S. Churio, C. M. Previtali, *Photochem. Photobiol. Sci.* **2004**, *3*, 960.
[6] K. Hoyer, U. Karsten, T. Sawall, C. Wiencke, *Mar. Ecol. Prog. Ser.* **2001**, *211*, 117.
[7] A. Gröniger, C. Hallier, D.-P. Häder, *J. Appl. Phycol.* **1999**, *11*, 437.
[8] A. Gröniger, R. P. Sinha, M. Klisch, D.-P. Häder, *J. Photochem. Photobiol., B* **2000**, *58*, 115.
[9] D. Schmid, C. Schürch, F. Zülli, *Cosmet. Toiletries Manuf. Worldwide* **2004**, 139.
[10] T. Misonou, J. Saitoh, S. Oshiba, Y. Tokitomo, M. Maegawa, Y. Inoue, H. Hori, T. Sakurai, *Mar. Biotechnol.* **2003**, *5*, 194.
[11] W. C. Dunlap, Y. Yamamoto, *Comp. Biochem. Physiol., B* **1995**, *112*, 105.
[12] J. M. Shick, W. C. Dunlap, *Ann. Rev. Physiol.* **2002**, *64*, 223.
[13] O. Holtkötter, T. Gerke, 'Kosmetische oder pharmazeutische Zubereitung zur Verbesserung der Sauerstoffaufnahme bei Menschen oder Tieren', DE 10259166 A1, 8-7-2004, Germany.
[14] W. P. Aue, E. Bartholdi, R. R. Ernst, *J. Chem. Phys.* **1975**, *64*, 2229; S. Braun, H.-O. Kalinowski, S. Berger, '150 and More Basic NMR Experiments', Wiley-VCH, Weinheim, 1998, p. 353.
[15] R. E. Hurd, *J. Magn. Reson.* **1990**, *87*, 422; M. von Kienlin, C. T. Moonen, A. van der Toorn, P. C. M. van Zijl, *J. Magn. Reson.* **1991**, *93*, 423; S. Braun, H.-O. Kalinowski, S. Berger, '150 and More Basic NMR Experiments', Wiley-VCH, Weinheim, 1998, p. 477.
[16] R. E. Hurd, B. K. John, *J. Magn. Reson.* **1991**, *91*, 648; W. Wilker, D. Leibfritz, R. Kerssebaum, W. Bermel, *Magn. Reson. Chem.* **1993**, *31*, 287; S. Braun, H.-O. Kalinowski, S. Berger, '150 and More Basic NMR Experiments', Wiley-VCH, Weinheim, 1998, p. 485.

[17] A. Bax, F. Summers, *J. Am. Chem. Soc.* **1986**, *108*, 2093; J. Ruiz-Cabello, G. W. Vuister, C. T. W. Moonen, P. van Gelderen, J. S. Cohen, P. C. M. van Zijl, *J. Magn. Reson.* **1992**, *100*, 282; S. Braun, H.-O. Kalinowski, S. Berger, '150 and More Basic NMR Experiments', Wiley-VCH, Weinheim, 1998, p. 489.
[18] S. Braun, H.-O. Kalinowski, S. Berger, '150 and More Basic NMR Experiments', Wiley-VCH, Weinheim, 1998, p. 460; K. Stott, J. Keeler, Q. N. Van, A. J. Shaka, *J. Magn. Reson.* **1997**, *125*, 302.
[19] D. Neuhaus, M. P. Williamson, 'The Nuclear Overhauser Effect in Structural and Conformational Analysis', 2nd edn., Wiley-VCH, New York, 2000.
[20] C. S. Johnson Jr., *Progr. Nucl. Magn. Reson. Spectrosc.* **1999**, *34*, 203; W. S. Price, *Concepts Magn. Reson.* **1997**, 299; W. S. Price, *Concepts Magn. Reson.* **1998**, 197.
[21] E. O. Stejskal, J. E. Tanner, *J. Chem. Phys.* **1965**, *42*, 288.
[22] A. D. Becke, *J. Phys. Chem.* **1993**, *97*, 5648; C. Lee, W. Yang, R. G. Parr, *Phys. Rev. B* **1988**, *37*, 785; P. J. Stephens, F. J. Devlin, C. F. Chabalowski, M. J. Frisch, *J. Phys. Chem.* **1994**, *98*, 11623; W. J. Hehre, L. Radom, P. v. R. Schleyer, J. A. Pople, 'Ab initio Molecular Orbital Theory', Wiley-Interscience, Wiley, New York, 1986.
[23] M. J. Frisch, G. W. Trucks, H. B. Schlegel, G. E. Scuseria, M. A. Robb, J. R. Cheeseman, J. A. Montgomery Jr., T. Vreven, K. N. Kudin, J. C. Burant, J. M. Millam, S. S. Iyengar, J. Tomasi, V. Barone, B. Mennucci, M. Cossi, G. Scalmani, N. Rega, G. A. Petersson, H. Nakatsuji, M. Hada, M. Ehara, K. Toyota, R. Fukuda, J. Hasegawa, M. Ishida, T. Nakajima, Y. Honda, O. Kitao, H. Nakai, M. Klene, X. Li, J. E. Knox, H. P. Hratchian, J. B. Cross, V. Bakken, C. Adamo, J. Jaramillo, R. Gomperts, R. E. Stratmann, O. Yazyev, A. J. Austin, R. Cammi, C. Pomelli, J. W. Ochterski, P. Y. Ayala, K. Morokuma, G. A. Voth, P. Salvador, J. J. Dannenberg, V. G. Zakrzewski, S. Dapprich, A. D. Daniels, M. C. Strain, O. Farkas, D. K. Malick, A. D. Rabuck, K. Raghavachari, J. B. Foresman, J. V. Ortiz, Q. Cui, A. G. Baboul, S. Clifford, J. Cioslowski, B. B. Stefanov, G. Liu, A. Liashenko, P. Piskorz, I. Komaromi, R. L. Martin, D. J. Fox, T. Keith, M. A. Al-Laham, C. Y. Peng, A. Nanayakkara, M. Challacombe, P. M. W. Gill, B. Johnson, W. Chen, M. W. Wong, C. Gonzalez, J. A. Pople, Gaussian 03, Revision C.02, Gaussian, Inc., Wallingford, CT, 2004.
[24] W. Koch, M. C. Holthausen, 'A Chemist's Guide to Density Functional Theory', Wiley-VCH, Weinheim, 2000; C. Dosche, M. U. Kumke, F. Ariese, A. N. Bader, C. Gooijer, P. I. Dosa, S. Han, O. S. Miljanic, K. P. C. Vollhardt, R. Puchta, N. J. R. van Eikema Hommes, *Phys. Chem. Chem. Phys.* **2003**, *5*, 4563; C. Dosche, M. K. Kumke, H.-G. Löhmannsröben, F. Ariese, A. N. Bader, C. Gooijer, O. S. Miljanic, M. Iwamoto, K. P. C. Vollhardt, R. Puchta, N. J. R. van Eikema Hommes, *Phys. Chem. Chem. Phys.* **2004**, *6*, 5476, and lit. cit. therein.
[25] A. C. Backes, J. Schatz and H.-U. Siehl, *J. Chem. Soc., Perkin Trans. 2* **2002**, 484.
[26] a) N. J. R. van Eikema Hommes, T. Clark, *J. Mol. Model.* **2005**, *11*, 175; b) R. Puchta, T. Clark, W. Bauer, *J. Mol. Model.* **2006**, *12*, 739.
[27] P. von Ragué Schleyer, C. Maerker, A. Dransfeld, H. Jiao, N. J. R. van Eikema Hommes, *J. Am. Chem. Soc.* **1996**, *118*, 6317; P. von Ragué Schleyer, H. Jiao, N. J. R. van Eikema Hommes, V. G. Malkin, O. L. J. Malkina, *J. Am. Chem. Soc.* **1997**, *119*, 12669; P. von Ragué Schleyer, M. Manoharan, Z.-X. Wang, B. Kiran, H. Jiao, R. Puchta, N. J. R. van Eikema Hommes, *Org. Lett.* **2001**, *3*, 2465; Z. Chen, C. S. Wannere, C. Corminboeuf, R. Puchta, P. von Ragué Schleyer, *Chem. Rev.* **2005**, *105*, 3842.
[28] Modgraph Consultants Ltd., http://www.modgraph.co.uk, Version 3.2.2.
[29] a) Y. Ding, K. Krogh-Jespersen, *Chem. Phys. Lett.* **1992**, *199*, 261; b) M. Knapp-Mohammady, K. J. Jalkanen, F. Nardi, R. C. Wade, S. Suhai, *Chem. Phys.* **1999**, *240*, 63.
[30] P. Skurski, M. Gutowski, R. Barrios, J. Simons, *Chem. Phys. Lett.* **2001**, *337*, 143.
[31] V. Raab, E. Gauchenova, A. Merkoulov, K. Harms, J. Sundermeyer, B. Kovacevic, Z. B. Maksic, *J. Am. Chem. Soc.* **2005**, *45*, 127; G. Bucher, *Angew. Chem.* **2003**, *115*, 4172; *Angew. Chem., Int. Ed.* **2003**, *42*, 4039, and lit. cit. therein.
[32] M. L. Hallensleben, H. Kansy, *Makromol. Chem* **1989**, *190*, 231; A. F. Pozharskii, *Uspekhi Khimii* **1998**, *67*, 3; H. A. Staab, T. Saupe, *Angew. Chem.* **1988**, *100*, 895; *Angew. Chem., Int. Ed.* **1988**, *27*, 865, and lit. cit. therein.
[33] R. Puchta, M. Galle, N. van Eikema Hommes, *Z. Naturforsch., B* **2006**, *61*, 1327.

[34] a) S. T. Howard, I. A. Fallis, *J. Org. Chem.* **1998**, *63*, 7117; b) Y. Miyahara, Y. Tanaka, K. Amimoto, T. Akazawa, T. Sakuragi, H. Kobayashi, K. Kubota, M. Suenaga, H. Koyama, T. Inazu, *Angew. Chem.* **1999**, *111*, 1008;*Angew. Chem., Int. Ed.* **1999**, *38*, 956.
[35] R. Schwesinger, *Angew. Chem.* **1987**, *99*, 1209; *Angew. Chem., Int. Ed.* **1987**, *11*, 1164; R. Schwesinger, M. Missfeldt, K. Peters, H. G. von Schnering, *Angew. Chem.* **1987**, *99*, 1210; *Angew. Chem., Int. Ed.* **1987**, *11*, 1165, and lit. cit. therein.
[36] Y. K. Lau, P. P. S. Saluja, P. Kebarle, R. W. Alder, *J. Am. Chem. Soc.* **1978**, *100*, 7328.
[37] Z. Zhang, Y. Tashiro, S. Matsukawa, H. Ogawa, *Fish. Sci.* **2005**, *71*, 1382.
[38] W. M. Bandaranayake, *Nat. Prod. Rep.* **1998**, *15*, 159.
[39] J. D. White, J. H. Cammack, K. Sakuma, G. W. Rewcastle, R. K. Widener, *J. Org. Chem.* **1995**, *60*, 3600; J. D. White, J. H. Cammack, K. Sakuma, *J. Am. Chem. Soc.* **1989**, *111*, 8970.
[40] A. Torres, C. D. Enk, M. Hochberg, M. Srebnik, *Photochem. Photobiol. Sci.* **2006**, *5*, 432.

Received October 31, 2006